



DEPARTMENT OF PHYSICS

TFY4561 - PHYSICS, PROJECT

Heat Control in Composite Overwrapped Pressure Vessels: Modeling and Simulation Approaches

Authors:

Abel G. Horneland
William Dugan

Bachelor project in physics

Supervisor Propulse NTNU: Even Drugli

Supervisor NTNU: Jon Andreas Støvneng

April, 2024

Abstract

A composite overwrapped pressure vessel being filled with high pressure gaseous nitrogen has been studied. As the tank is filled, the internal energy of the gas increases, which in turn heats up the tank wall. The outermost wall layer loses its strength when heated far above 65 °C. The goal is to find out how quickly the tank can be filled without exceeding this limit.

A custom simulator is implemented in C++ to perform rapid simulations of the process. The simulator can switch between different one-dimensional thermal models, including a thermal resistance model and a finite difference model. The resistance model fails to give accurate results, which is due to the transient nature of the system being simulated. The FDM model is a more suitable approach to apply as it separates the thin tank wall into smaller layers, and can be easily extended to two dimensions. A previously developed mass flow model is used in order to simulate mass transfer from two supply tanks, with initial pressures of 200 bars and 300 bars respectively. In order to extend the basis for comparison between models, a third model was developed using Simulink Simscape Fluids.

Physical testing was performed in order to both fine-tune physical parameters in the simulation, as well as to gather empirical data for comparison with the three different numerical models. The results showed that the finite difference model most accurately predicts the outer wall temperature. The Simulink model fills the tanks slower and undershoots the temperature, while the resistance model significantly overshoots the heat transfer through the wall during the transient filling. It was not possible to quantitatively determine the accuracy of the simulated gas temperatures and inner wall temperatures, as the measurements of the gas temperature from testing showed to be wrong, whilst it was not practically possible to place a temperature sensor on the inner wall of the tank.

The empirical data showed that the wall temperature does not reach above the limit of 65 °C during the filling process by using carefully chosen restriction orifices. This result is also predicted accurately by the finite difference model, meaning it can be utilized to simulate Propulse NTNU's future systems only requiring minor improvements.

Sammendrag

En *composite overwrapped pressure vessel* fylt med nitrogengass på høyt trykk har blitt studert. Når tanken fylles, øker den indre energien til gassen, noe som igjen varmer opp tankveggen. Det ytterste veggslaget mister sin styrke når det oppvarmes forbi 65 °C. Målet til oppgaven er å finne ut hvor raskt tanken kan fylles uten å overstige denne grensen.

En skreddersydd simulator er implementert i C++ for å utføre simuleringer av prosessen. Simulatoren kan veksle mellom ulike éndimensjonale termiske modeller, inkludert en termisk motstandsmodell og en endelige differanse metode (FDM). Motstandsmodellen gir ikke nøyaktige resultater, noe som skyldes at systemet som blir simulert er i raske transiente. FDM-modellen er en mer egnet tilnærming å bruke da den deler den tynne tankveggen inn i mindre lag, og kan enkelt utvides til to dimensjoner. En tidligere utviklet massestrømsmodell brukes for å simulere masseoverføring fra to forsyningstanker, med starttrykk på henholdsvis 200 bar og 300 bar. For å utvide grunnlaget for sammenligning mellom modellene, ble det utviklet en tredje modell ved hjelp av Simulink Simscape Fluids.

Fysiske tester ble utført både for å finjustere fysiske parametere i simuleringen og for å samle empiriske data for sammenligning med de tre ulike numeriske modellene. Resultatene viste at FDM-modellen mest nøyaktig forutsier ytterveggtemperaturen. Simulink-modellen fyller tankene tregere og underestimerer temperaturen, mens motstandsmodellen overestimerer varmeoverføringen gjennom vegg under den transiente fyllingen. Det var ikke mulig å kvantitativt bestemme nøyaktigheten av simulerte gastemperaturer og indre veggtretemperaturer, ettersom målingene av gastemperaturen fra testing viste seg å være feil, samtidig som det ikke var praktisk mulig å plassere en temperatursensor på den indre veggan av tanken.

De empiriske dataene viste at veggetemperaturen ikke når over grensen på 65 °C under fyllingsprosessen ved å bruke nøyne valgte begrensningsdyser. Dette resultatet forutsies også nøyaktig av FDM-modellen, noe som betyr at den kan brukes til å simulere Propulse NTNU's fremtidige systemer med bare mindre forbedringer.

Preface

This bachelor thesis serves as the final project for a 3-year study programme leading to a Bachelor's degree in Physics at the Norwegian University of Science and Technology. The task is provided by Propulse NTNU. It is written as an independent project in a group of two students, with guidance from both Propulse NTNU and the Department of Physics.

We want to thank our supervisors, Jon Andreas Støvneng, for helping us figure out how to approach the problem and for encouraging the project, and Even Drugli for sharing his testing expertise, and guiding us in writing the thesis report.

We also want to thank Propulse NTNU for investing resources into the project and allowing us the use of their equipment for testing our models. Their guidance has taught us much about the practical applications of physics, and how to write sustainable code. We especially want to thank Ola and Anders for helping us solve numerous issues with our code, despite not fully understanding the underlying physics.

Table of Contents

Glossary	vi
Acronyms	vi
1 Introduction	1
1.1 High pressure COPV	1
1.2 System overview	2
2 Theory	3
2.1 Adiabatic compression of an ideal gas	3
2.2 Steady state heat transfer	3
2.2.1 Thermal resistances	4
2.2.2 Finite differences	5
2.3 Restriction orifices	6
2.4 Time discretization	7
2.4.1 Adiabatic compression	7
2.4.2 Thermal resistances	7
2.4.3 Finite differences	8
3 Simulation methods	10
3.1 Custom simulator	11
3.2 Simulink Simscape Fluids	13
4 Model verification	16
4.1 Equipment	16
4.2 Contact resistance	17
4.3 Filling tests	18
5 Results	20
5.1 Ideal simulation results	20
5.1.1 Thermal resistances	20

5.1.2	FDM	21
5.1.3	Simulink Simscape Fluids	22
5.2	Test results	23
5.2.1	Contact resistance	23
5.2.2	Filling test	24
6	Discussion	26
6.1	Numerical model comparison	26
6.2	Numerical simulations	28
6.3	Contact resistance test	28
6.4	Filling test	28
7	Conclusion	30
Bibliography		31
Appendix		32
A Wall area estimation		32

Glossary

Check valve One-way directional flow valve.

Solenoid valve Valve controlled by an electromagnet.

Thermocouple Temperature sensor using the Seebeck effect.

Acronyms

ADC Analog to digital converter.

COPV Composite overwrapped pressure vessel.

DAQ Data acquisition.

FDM Finite difference method.

HP High pressure (300 bar).

LP Low pressure (200 bar).

P&ID Piping and instrumentation diagram.

PT Pressure transducer.

TDC Thermocouple to digital converter.

1 Introduction

When filling a gas tank, the internal pressure increases quickly from atmospheric pressure to high working pressures, commonly 300 bars or 700 bars in aerospace applications. This increase in pressure results in increased internal energy of the gas, which dissipates into the tank wall.

Propulse NTNU develops liquid rocket propulsion systems and routinely fills its tanks with high pressure gaseous nitrogen. The filling process must take several practical constraints into account. The filling process involves allowing gas from one or more supply tanks to flow into the rocket tank. Given the time-sensitive nature of rocket launches, the entire filling process must be completed within 10 minutes. Furthermore, the outer wall temperature must be kept within its designed limits throughout the process.

Previous studies have investigated the filling of gaseous hydrogen vessels for transportation applications [1]. Although this thesis focuses on gaseous nitrogen, parallels between both the simulation methods and results will be drawn.

1.1 High pressure COPV

Developing a tank capable of containing hundreds of bars of internal pressure is a significant challenge. Using only metallic materials would require thick walls, which is not a suitable solution in aerospace due to weight constraints. Incorporating composite materials into the design offers a viable solution to this challenge.

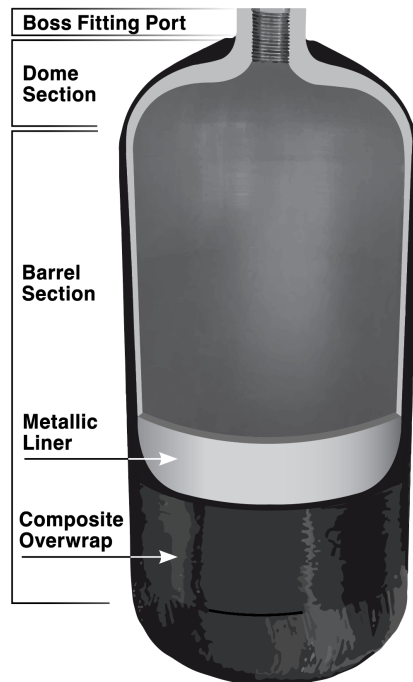


Figure 1: Cross-sectional view of a COPV. [2]

A tank that utilises both metallic and composite materials is referred to as a composite overwrapped pressure vessel (COPV). A COPV is depicted in Figure 1. COPVs consist of two layers: a non-structural aluminum liner that defines the shape and separates the fluid from the composites, and a structural fiber composite layer that holds the pressure. The composite layer is made by wrapping the liner in continuous fibers, either glass- or carbon fibers, before it is solidified in epoxy. Since the fibers are thin, many layers are required to give a total layer thickness of a few millimeters. Note that COPVs must have its connections placed along the center axis, meaning the tank can have either one or two connections.

1.2 System overview

The system depicted in Figure 2 comprises two supply tanks, one receiver tank (the COPV), and several valves and sensors. The COPV is designed, manufactured, and tested according to ISO 11119-2:2020.[3] It has a volume of 6.8 liters and a working pressure of 310 bars at 65 °C.

Each supply tank is a steel cylinder provided by a gas distributor, with a volume of 50 liters. One supply tank, designated as the low-pressure supply (LP), has a pressure of 200 bars, while the other, designated as the high-pressure supply (HP), has a pressure of 300 bars.

The decision to use both LP and HP stems from the fact that LP bottles are significantly less expensive than HP bottles. This allows for cost-effective filling, done sequentially to optimize resources and expenses.

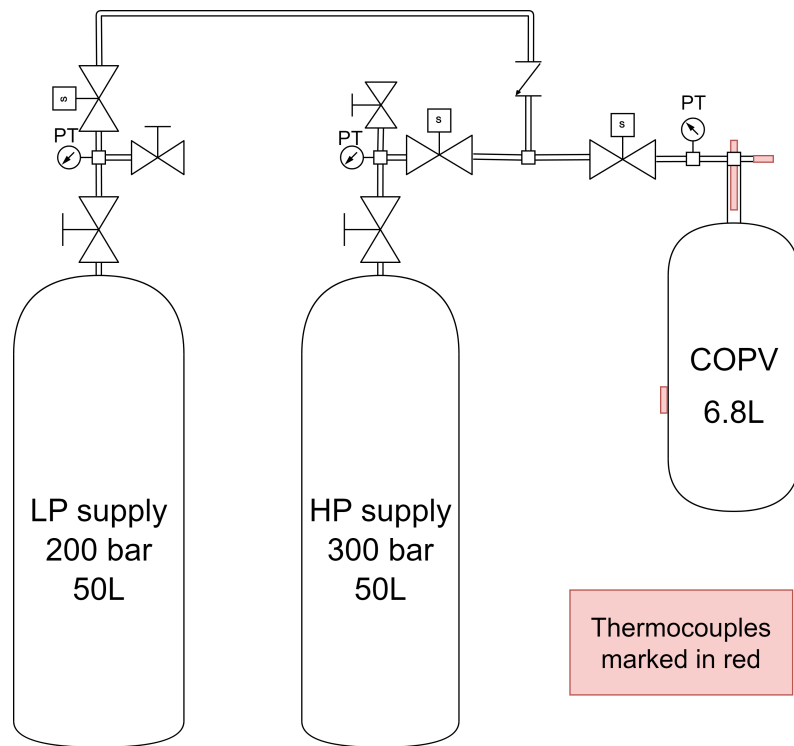


Figure 2: P&ID.

2 Theory

2.1 Adiabatic compression of an ideal gas

The gas is modelled as an ideal gas, with an equation of state

$$PV = mR_s T, \quad (1)$$

where P is pressure, V is volume, m is mass, and T is the absolute temperature. R_s is the specific gas constant given by

$$R_s = \frac{R}{M_{\text{gas}}}, \quad (2)$$

where R is the universal gas constant and M_{gas} is the molar mass of the gas. The adiabatic relations are

$$PV^\gamma = \text{constant}, \quad (3a)$$

$$P^{\gamma-1}/T^\gamma = \text{constant}, \quad (3b)$$

$$\gamma = c_P/c_V. \quad (3c)$$

Here, c_P and c_V are the specific heat capacities under constant pressure and volume. Let subscript 1 and 2 be the gas state before and after an adiabatic process occurs, respectively. This thesis will only consider a constant volume tank, thus $V_2/V_1 = 1$. The pressure after the process is then

$$P_2 = P_1 \left(\frac{m_2}{m_1} \right)^\gamma, \quad (4)$$

and the temperature is

$$T_2 = T_1 \left(\frac{m_2}{m_1} \right)^{\gamma-1}. \quad (5)$$

When the mass inside the tank is increased, one can observe that both the pressure and the temperature increases accordingly.

2.2 Steady state heat transfer

Since the inner diameter of the tank is large proportionally to the wall thickness, a good first approximation is a 1-dimensional model. The material of each wall layer is assumed to be homogeneous, and independent from the temperature of the layer. The surface area A of the tank used in the model is approximated in Appendix A.

Fourier's law in one dimension is given in differential form by

$$q = -\kappa \frac{dT}{dx} \quad (6)$$

where q is the heat flux density and κ is the thermal conductivity. By assuming a steady state heat flow, $dq/dt = 0$, dT/dx is constant. The result is a linear drop in

temperature through the wall. Let L be the thickness in the direction parallel to the heat flow. Then the heat flux is

$$\dot{Q} = qA = -\kappa A \frac{\Delta T}{L}. \quad (7)$$

Equation (7) describes the conductive heat transfer in the wall layers. On either side of the wall, namely the inner and outer boundary, the wall is subject to convection. The convective heat flow is given by Newton's law of cooling,

$$\dot{Q} = hA\Delta T. \quad (8)$$

Here, \dot{Q} is the heat flux out of the wall, h the heat transfer coefficient and A the surface area. ΔT is different for the inner and outer boundary. On the outer boundary, ΔT denotes the difference between the outer wall temperature and the temperature of the environment. On the inner boundary, ΔT is the difference between the gas temperature and the inner wall temperature.

2.2.1 Thermal resistances

For each layer in the wall, one can define a thermal resistance, R , as the ratio between the layer's temperature drop, ΔT , and the heat flux,

$$R = \frac{\Delta T}{\dot{Q}}. \quad (9)$$

The total thermal resistance is given as the ratio between the temperature drop across the entire wall and the heat flow,

$$R_{\text{total}} = \frac{\Delta T_{\text{total}}}{\dot{Q}}. \quad (10)$$

Since the total temperature drop across the wall is equal to the sum of the temperature drops in each layer, the total thermal resistance is the sum of the resistance in each layer. Rearranging equation (10) gives an expression for the heat flow,

$$\dot{Q} = \frac{T_g - T_{\text{amb}}}{R_{\text{total}}}, \quad (11)$$

where T_g is the gas temperature. The component resistances are visualized in Figure 3. By using equation (9),

$$R_{\text{convective},g} = \frac{1}{h_g A}, \quad (12a)$$

$$R_{\text{liner}} = \frac{L_{\text{liner}}}{A\kappa_{\text{liner}}}, \quad (12b)$$

$$R_{\text{wrapping}} = \frac{L_{\text{wrapping}}}{A\kappa_{\text{wrapping}}}, \quad (12c)$$

$$R_{\text{convective},o} = \frac{1}{h_o A}. \quad (12d)$$

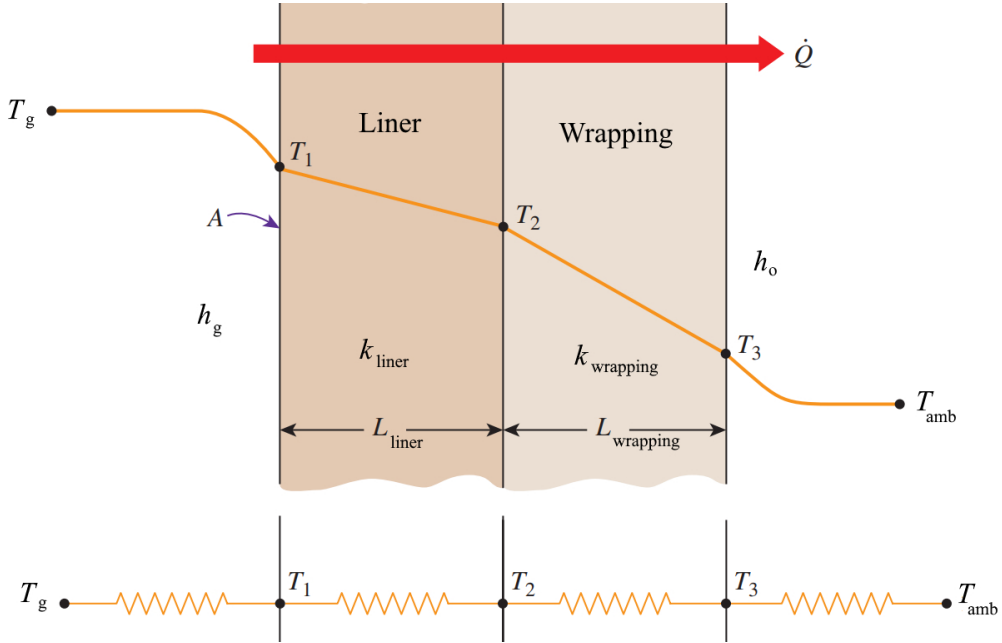


Figure 3: Cross-sectional view of the tank wall. Adapted from [4].

Here, h_g and h_o is the heat transfer coefficients of the gas and air outside the tank, L_{liner} and L_{wrapping} the wall layer thickness, with thermal conductance κ_{liner} and κ_{wrapping} , respectively. Since interface between the liner and overwrap is imperfect, a thermal resistance is introduced between the layers. This contact resistance, R_{contact} , has to be found experimentally, which is detailed in section 4.2. The total thermal resistance of the system is

$$R_{\text{total}} = R_{\text{convective},g} + R_{\text{liner}} + R_{\text{contact}} + R_{\text{wrapping}} + R_{\text{convective},o}. \quad (13)$$

The total heat flow given in equation (11) will be distributed to the different wall layers, analogous to a current through resistances in series. Two temperatures are needed to calculate the entire temperature profile. The ambient temperature is known, and one can use equation (5) in order to approximate the gas temperature. This gives the following temperature profile:

$$T_1 = T_g - \dot{Q}R_{\text{convective},g}, \quad (14a)$$

$$T_2 = T_g - \dot{Q}(R_{\text{convective},g} + R_{\text{liner}}), \quad (14b)$$

$$T_3 = T_g - \dot{Q}(R_{\text{convective},g} + R_{\text{liner}} + R_{\text{contact}} + R_{\text{wrapping}}), \quad (14c)$$

where T_i are in accordance to Figure 3.

2.2.2 Finite differences

In the previous section, the wall was only split up into its physical layers. To improve the thermal model, each layer will be subdivided into smaller intervals. Such a technique is called a finite difference method (FDM), where the time domain is discretized in order to approximate derivatives. Thus, for each time step, the heat equation will be solved in the spatial domain.

To approximate spatial derivatives, a finite set of elements will be generated, with each element's center points referred to as nodes. The solution will only be valid in the nodes, thus it is essential to use a high enough resolution for a convergent solution. The volume of each element is defined as $dxdydz \rightarrow \Delta x \Delta y \Delta z$. Using the same surface area as the previous model, $\Delta x \Delta y \Delta z = A \Delta x$. It is convenient to make the two boundary elements have width $\Delta x/2$, since the nodes then get positions 0, Δx , $2\Delta x$, etc.

Given the discrete nature of this method in both time and space, further discussion will be provided in section 2.4.

2.3 Restriction orifices

There are multiple ways of determining the mass flow through the valves. Most methods use isentropic flow as a base assumption. A common source is the formulae given in ISO 5167-1 [5], however these only apply to steady, single-phase, subsonic flow. Due to the transient nature of the system being modelled, another approach is needed. Section 2.5.2.3 in [6] describes single-phase flow through an orifice, both sonic and subsonic. Although the source does not offer a direct derivation of the equations included in this thesis, they will be adopted without explicit proof, as the focus lies on thermal modeling. The mass flow is given by

$$\dot{m} = C_d A \psi \sqrt{\rho_1 P_1 \gamma \left(\frac{2}{\gamma + 1} \right)^{(\gamma+1)/(\gamma-1)}} \quad (15)$$

where C_d is a dimensionless discharge coefficient, A is the smallest cross-sectional area within the flow passage, ψ is a dimensionless constant, ρ_1 is the upstream density, and P_1 is the upstream pressure. C_d is determined by the geometry of the restriction and is between 0 and 1. The flow is critical when

$$\frac{P_1}{P_2} \geq \left(\frac{\gamma + 1}{2} \right)^{\gamma/(\gamma-1)} \quad (16)$$

where P_2 is the downstream pressure. In the case of critical flow, $\psi = 1$. If the flow is subsonic (not critical), then

$$\psi^2 = \frac{2}{\gamma - 1} \left(\frac{\gamma + 1}{2} \right)^{(\gamma+1)/(\gamma-1)} \left(\frac{P_1}{P_2} \right)^{2/\gamma} \left[1 - \left(\frac{P_1}{P_2} \right)^{(\gamma-1)/\gamma} \right]. \quad (17)$$

2.4 Time discretization

2.4.1 Adiabatic compression

Let Δt be the discrete time step. The mass added during the time step is

$$\dot{m}_k = \dot{m}(\rho_k, P_k), \quad (18a)$$

$$m_{k+1} = m_k + \dot{m}_k \Delta t, \quad (18b)$$

where \dot{m} is given by equation (15). The increased mass yields an increase in both pressure and temperature,

$$P_{k+1} = P_k \left(\frac{m_{k+1}}{m_k} \right)^\gamma, \quad (19a)$$

$$T_{k+1} = T_k \left(\frac{m_{k+1}}{m_k} \right)^{\gamma-1}. \quad (19b)$$

Here, $k = 0, 1, \dots$ represent the discrete times $t_k = k\Delta t$. The density follows from equation (1),

$$\rho_{k+1} = \frac{P_{k+1}}{R_s T_{k+1}}. \quad (20)$$

2.4.2 Thermal resistances

The total heat transfer is

$$\dot{Q}_k = \frac{T_k^g - T_{\text{amb}}}{R_{\text{total}}} \quad (21)$$

where T_k^g is the gas temperature in time step k . The resulting temperature distribution is

$$T_{k+1}^1 = T_k^g - \dot{Q}_k R_{\text{convective},g} \quad (22a)$$

$$T_{k+1}^2 = T_k^g - \dot{Q}_k (R_{\text{convective},g} + R_{\text{liner}}) \quad (22b)$$

$$T_{k+1}^3 = T_k^g - \dot{Q}_k (R_{\text{convective},g} + R_{\text{liner}} + R_{\text{wrapping}}). \quad (22c)$$

To model the temperature change of the gas, one can consider the change in internal energy,

$$\frac{dU}{dt} = c_V \frac{d}{dt}(mT) = mc_V \frac{dT}{dt} + c_V T \frac{dm}{dt}. \quad (23)$$

Since the internal energy of a system is extensive, an increase in internal mass yields an increase in internal energy [7]. By approximating the time derivatives, the change in internal energy is

$$\frac{\Delta U}{\Delta t} = m_k c_V \left[\frac{T_{k+1}^g - T_k^g}{\Delta t} \right] + c_V T_k^g \dot{m}_k. \quad (24)$$

Note that the choice of time indices outside of the differentials determine if the method is implicit or explicit. An explicit solution is chosen for simplicity. Since

the volume is constant, no work is being done on the gas. Thus, $\Delta U/\Delta t = -\dot{Q}_k$, and the expression for T_{k+1}^g becomes

$$T_{k+1}^g = T_k^g - \frac{Q_k}{m_k c_v} + \Delta t \frac{\dot{m}_k}{m_k} T_k^g. \quad (25)$$

The pressure follows from equation (1).

2.4.3 Finite differences

Assume a solution $T_k = T(x, t = k\Delta t)$ is known and let $n \in \mathbb{N}$ such that $n\Delta x \in (0, L)$ where L is the total wall thickness. This represents an internal node, meaning the centre point of an element not subjected to boundary conditions. The heat flow through a node is

$$\dot{Q} = m c_V \frac{dT^n}{dt} \quad (26)$$

which is approximated by

$$\dot{Q} = \rho A \Delta x c_V \left[\frac{T_{k+1}^n - T_k^n}{\Delta t} \right] \quad (27)$$

where the mass is substituted by $m = \rho V = \rho A \Delta x$. There is no convection for these nodes, only conduction. Heat flowing into the node is defined as positive. Thus, by using (7),

$$\begin{aligned} \dot{Q} &= \dot{Q}_{\text{conduction,in}} + \dot{Q}_{\text{conduction,out}} \\ &= \kappa A \left[\frac{T_{k-1}^{n-1} - T_k^n}{\Delta x} \right] - \kappa A \left[\frac{T_k^{n+1} - T_k^n}{\Delta x} \right] \\ &= \frac{\kappa A}{\Delta x} [T_{k-1}^{n-1} - 2T_k^n + T_k^{n+1}]. \end{aligned} \quad (28)$$

With the current mesh, the conductivity is now a function of position. By using equation (27), the expression for T_{k+1}^n is

$$\begin{aligned} T_{k+1}^n &= T_k^n + \frac{\kappa \Delta t}{\rho c_V (\Delta x)^2} [T_{k-1}^{n-1} - 2T_k^n + T_k^{n+1}] \\ &= T_k^n + \alpha(n) \frac{\Delta t}{(\Delta x)^2} [T_{k-1}^{n-1} - 2T_k^n + T_k^{n+1}], \end{aligned} \quad (29)$$

where $\alpha = \kappa / (\rho c_V)$ is the thermal diffusivity. Consider now an $N \in \mathbb{N}$ such that $N\Delta x = L$. This is the node on the outside of the tank. It experiences conduction from the left and convection from the right. Thus,

$$\begin{aligned} \dot{Q} &= \dot{Q}_{\text{conduction,in}} + \dot{Q}_{\text{convection,out}} \\ &= \kappa A \left[\frac{T_{k-1}^{N-1} - T_k^N}{\Delta x} \right] - h_o A [T_k^N - T_{\text{amb}}] \end{aligned} \quad (30)$$

where equation (8) is used for $\dot{Q}_{\text{convection,out}}$. The expression for T_{k+1}^N is then

$$T_{k+1}^N = T_k^N + 2\alpha(N) \frac{\Delta t}{(\Delta x)^2} [T_{k-1}^{N-1} - T_k^N] - \frac{2h_o \Delta t}{\rho c_V \Delta x} [T_k^N - T_{\text{amb}}]. \quad (31)$$

The factor of two in the two last terms come from the $\Delta x/2$ element width. Consider now the internal boundary node, T_{k+1}^0 . It experiences convection from the gas to the left and conduction with the neighbouring node to the right. The heat flow is

$$\begin{aligned}\dot{Q} &= \dot{Q}_{\text{convection,in}} + \dot{Q}_{\text{conduction,out}} \\ &= h_i A [T_k^g - T_k^0] - \kappa A \left[\frac{T_k^0 - T_k^1}{\Delta x} \right],\end{aligned}\tag{32}$$

which gives a temperature

$$T_{k+1}^0 = T_k^0 + \frac{2h_i \Delta t}{\rho c_V \Delta x} [T_k^g - T_k^0] - 2\alpha(0) \frac{\Delta t}{(\Delta x)^2} [T_k^0 - T_k^1].\tag{33}$$

The gas temperature is given by equation (25) where \dot{Q} is the convection term in equation (32). The pressure follows from equation (1).

In his paper on numerical stability for thermal analysis, Lee [8] showed that the required time step for a stable solution of the diffusion equation using FDM is

$$\frac{\Delta t}{(\Delta x)^2} \leq \frac{1}{2} \frac{1}{\max_{x \in [0,L]}(\alpha)}.\tag{34}$$

This does not account for the convective boundaries, thus a pessimist factor $C \in (0, 1]$ is added,

$$\Delta t = \frac{C(\Delta x)^2}{2 \max_{x \in [0,L]}(\alpha)}.\tag{35}$$

3 Simulation methods

In this section, various methods for simulating the pressure and temperature inside the tank during the filling process will be explored. To ensure the comparability of the models, the following criteria has been set:

- **Completeness:** All components of the physical system must be included in all models.
- **Consistency:** All physical constants and properties must be the same throughout all models. See Table 1.
- **Stability:** For numerical methods, the step size must be sufficiently small to ensure a stable solution.

Table 1: Physical properties used for simulations.

Parameter	Symbol	Value	Source
Ambient temperature	T_{amb}	20 °C	
Tank surface area	A	0.29 m ²	Appendix A
Heat transfer coefficient gas	h_g	200 W/(m ² K)	[4]
Heat transfer coefficient air	h_o	10 W/(m ² K)	[4]
Aluminium liner			
Density	ρ	2700 kg/m ³	[1]
Specific heat	c_V	896 J/(kgK)	[1]
Conductivity	κ	167 W/(mK)	[1]
Thickness	L	2 mm	
Carbon fiber wrapping			
Density	ρ	1790 kg/m ³	Estimate based on [1], [4], [9]
Specific heat	c_V	1000 J/(kgK)	Estimate based on [1], [4], [9]
Conductivity	κ	0.5 W/(mK)	Estimate based on [1], [4], [9]
Thickness	L	4.5 mm	
Nitrogen gas			
Specific heat	c_V	1040 J/(kgK)	[4]
Gas constant	R_s	296.8 J/(kgK)	[4]
Isentropic exponent	γ	7/5	[7]

3.1 Custom simulator

A custom simulation program has been implemented in C++ and includes the different models described in section 2.4. An overview is given in Figure 4.

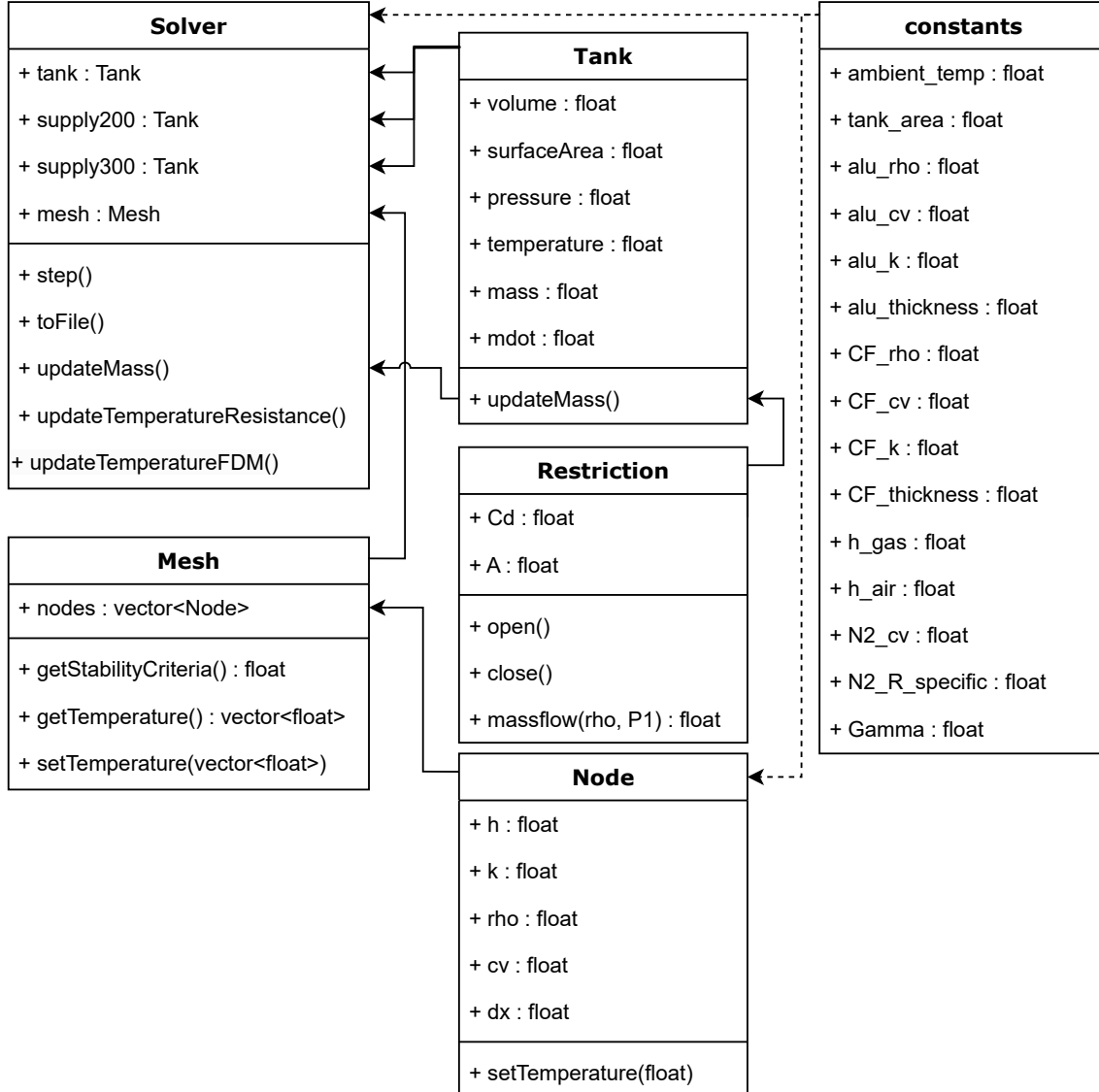


Figure 4: Class diagram for the object oriented simulation program.

The simulation program models the two supply tanks as isentropic volumes. Each supply tank is connected to a restriction which can open and close, which in turn is connected to the simulated COPV. The pipes connecting the supply tanks, restrictions and COPV are modeled as if they are isentropic and lossless, meaning there is no heat loss and no pressure drop across the pipes.

The solver controls the simulation. It starts with the LP supply open and the HP supply closed, and swaps supplies when the pressure in the COPV is within one bar of the LP supply. The HP supply is also closed once pressure in the COPV is within one bar, thus the COPVs gas mass remains constant after the filling is completed.

For each time step, the solver calculates the mass flow using the isentropic mass flow model given in 2.4. The solver then subtracts the mass flowing through the restriction from the supply tank's gas mass, and adds it to the COPV's gas mass. After this has occurred, the pressure and temperature will change according to the adiabatic model for both the supply tank and the COPV. The compression of the gas is approximated as adiabatic because the compression and heating of the gas in the transient filling phase is a much faster process than the heat transfer from the gas through the wall.

The thermal model for the wall is applied after the mass has increased. The temperature profile through the wall is then found through one of the different models. If the gas temperature decreases under constant mass conditions, the pressure will decrease accordingly. The following thermal models have been implemented:

- **Mode 0:** This mode keeps all temperatures constant and equal to the ambient temperature.
- **Mode 1:** Thermal resistance model as described in section 2.4.2. A convective boundary condition is applied to the outer wall.
- **Mode 2:** FDM model as described in section 2.4.3. An adiabatic boundary condition is applied to the outer wall by setting $h_o = 0$.
- **Mode 3:** FDM model as described in section 2.4.3 with a convective outer boundary.
- **Other modes:** Heat transfer through the wall can be disabled completely. This yields an adiabatic compression of the gas inside the tank.

Once the mass flow and heat flow calculations have been done, the solver checks if any of the valves should change from opened to closed or vice versa. The simulation is run for 600 seconds to see how the pressures and temperatures develop after the filling process is complete.

3.2 Simulink Simscape Fluids

Simulink has an additional package for block-programmed simulations named Simscape. It includes sub-packages for liquid, gas, hydraulic and electronic systems. By using these blocks, it is possible to model complex systems with multiple parts. Simulink code is written in the MATLAB language and one can access all source code for the blocks, giving full control and insight of the model. Diagrams in Simulink are usually read left-to-right.

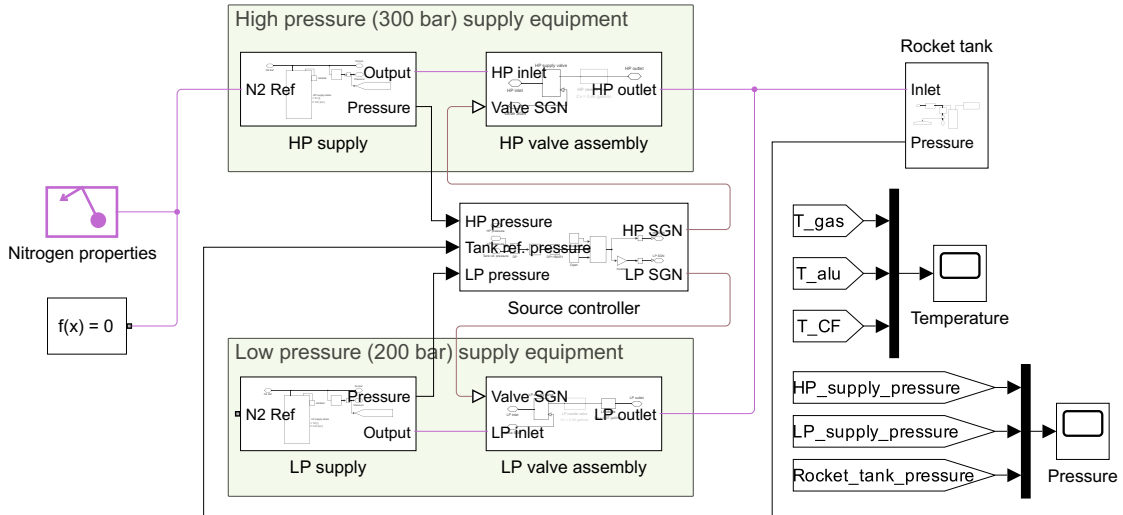


Figure 5: Overview of the Simulink Simscape Fluids model.

The overview in Figure 5 shows a similar setup to what is described in the P&ID. There are two gas supply tanks and the source controller determines when each of the supply valves are open. The HP and LP gas pressures are sent to the source controller.

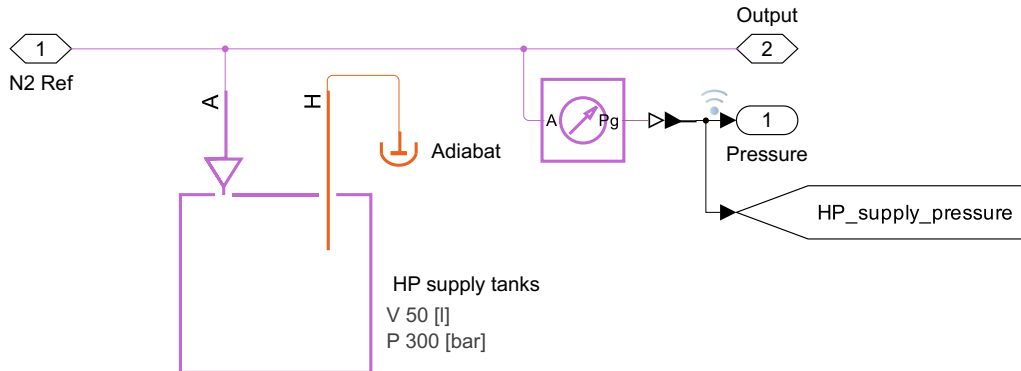


Figure 6: HP and LP tank subsystems.

The valve assemblies are also similar for HP and LP, but the LP includes a check valve. Note that the valves are opened or closed in this model, with a response time of approximately 25 ms.

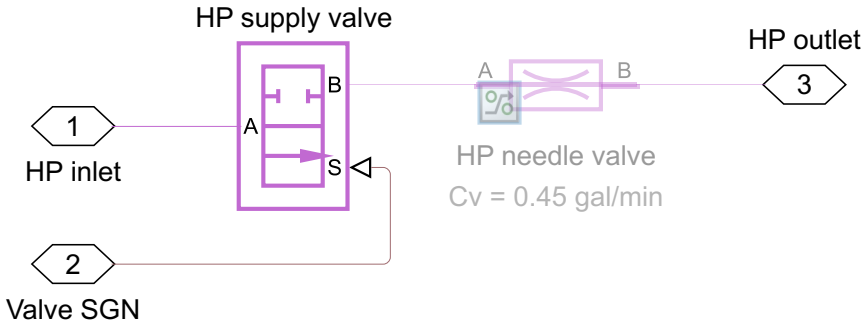


Figure 7: HP and LP valve subsystems.

The source controller performs the following logic:

- Start by filling from LP.
- When the pressure difference between the rocket tank and LP reaches one bar, stop filling from LP and start filling from HP.
- When the pressure difference between the rocket tank and HP reaches one bar, or 10 minutes elapse, stop filling from HP.

The source controller is modelled as an analogue circuit, but during testing the logic will be performed digitally. The rocket tank valve is always open, hence it is modelled as a constant restriction. The tank sends its internal pressure back to the source controller with a feedback loop.

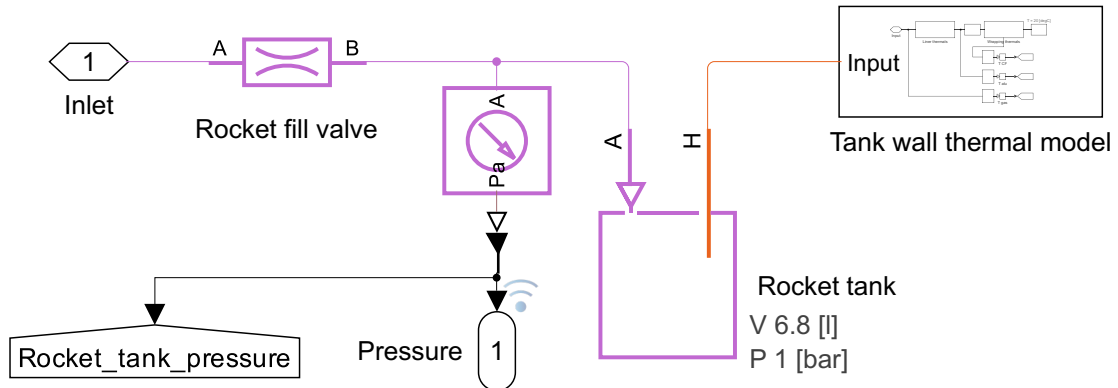


Figure 8: Rocket tank model.

A custom block for the tank wall thermal properties has been made. This simple block includes all the thermal properties needed to estimate the heat flow through the tank wall. Note that the wall is one-dimensional with an area normal to the heat flow equal to the total tank surface area. There are temperature sensor blocks that send the measured gas and wall temperatures back to the top layer resulting scope, which produce a graph of the results. The rightmost block is a temperature reference where the ambient temperature is set. The thermal model can be seen in figures 9 and 10.

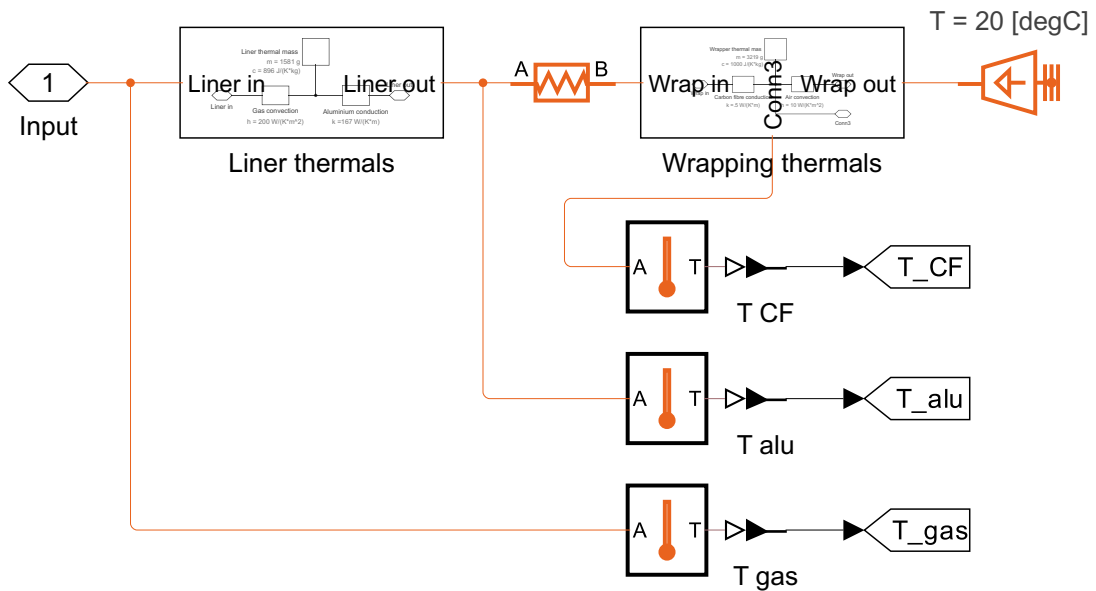


Figure 9: Rocket tank thermal model.

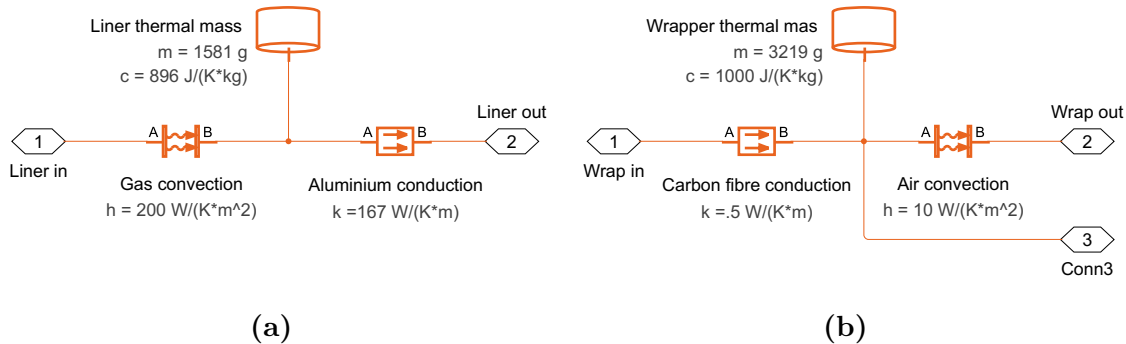


Figure 10: (a) Thermal model going from the inside of the rocket tank and through the aluminium liner to the middle boundary. (b) Thermal model going from the middle boundary through the wrapping to the ambient air.

Simulink will automatically adjust the time step according to user set absolute and relative errors and will therefore be considered stable without further detail.

4 Model verification

Physical testing with the COPV was conducted to gather empirical data and validate the simulation models. Two tests were performed: one to determine the thermal contact resistance between the liner and wrapping, and another filling test where the tank was filled in a manner consistent with the simulations developed earlier.

4.1 Equipment

The tests were performed using Propulse NTNU's data acquisition system (DAQ). It is a system for reading sensor data and controlling valves in the rocket's propulsion system during testing and launch. In order to read data from the sensors listed in Table 2, the DAQ uses the MAX31856 TDC to measure the temperature and the ADS8678 ADC to measure the pressure. The DAQ is also responsible for controlling the solenoid valves that control the filling of the tank.

Table 2: Description of the components used for model verification testing.

Part	Model numer	Comment
Tank	Vestteknikk 6.8L	
Thermocouple	Therma LT-1-3000-K-KFD30-S-0	Surface temperatures
Thermocouple	Therma EST-53023-S-10-G1/4"	Gas temperature, ambient temperature
Thermocouple	Therma EST-53023-S-100-G1/4"	Gas temperature, 100 mm long probe
Pressure sensor	SICK PBT-RB400SG1SENUMA0Z	Gas pressures
Solenoid valve	Jaksa 320827	Controls gas flow from LP and HP supply
Check valve	Swagelok SS-CHS4-1	Prevents flow from HP into LP supply.

4.2 Contact resistance

The contact resistance between the liner and the overwrap has to be found experimentally. An illustration of the test setup used to measure the temperatures is shown in Figure 11. The COPV was circulated with hot water at a constant temperature. One thermocouple was mounted inside the water stream and one thermocouple was mounted on the outer wall. It was not possible to mount a thermocouple to the inner wall, yet this would have given valuable data. The ambient temperature was measured with a third thermocouple. After the COPV reached a steady state, temperature data was collected for 90 seconds while still circulating the hot water.

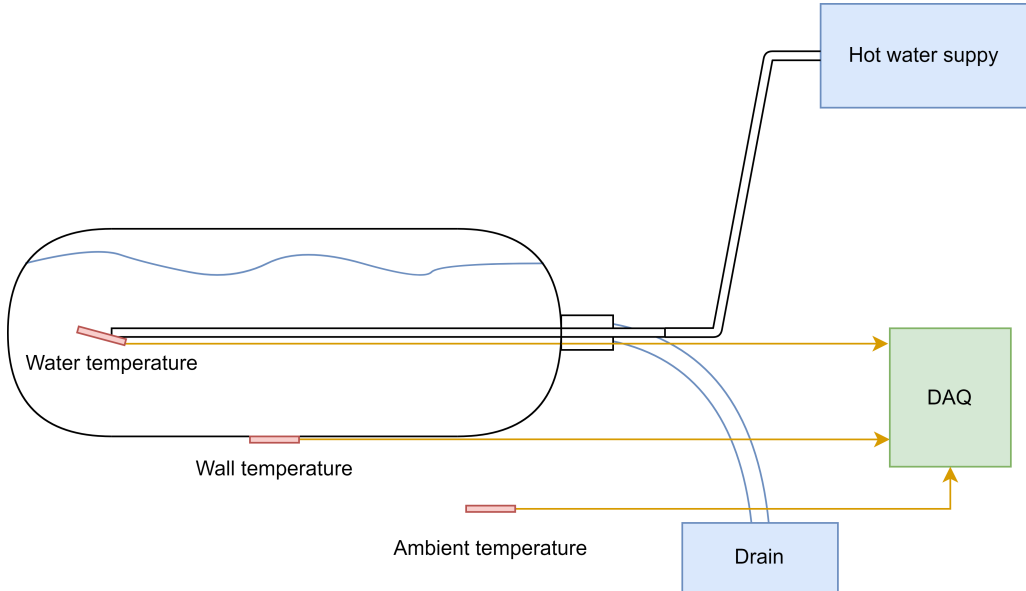


Figure 11: Illustration of the test setup used to find the contact resistance of the COPV.

The contact resistance can be calculated using

$$\min_{R_{\text{contact}}} T_{\text{water}} - T_{\text{wall}} - \dot{Q}(R_{\text{water}} + R_{\text{liner}} + R_{\text{contact}} + R_{\text{wrapping}}) \quad (36)$$

where

$$\dot{Q} = \frac{T_{\text{water}} - T_{\text{amb}}}{R_{\text{water}} + R_{\text{liner}} + R_{\text{contact}} + R_{\text{wrapping}} + R_{\text{convective},o}}. \quad (37)$$

Here, R_{water} is the resistance at the water-liner boundary and comes from the heat transfer coefficient for forced convection of water, which is estimated to be $h_{\text{water}} = 1000 \text{ W}/(\text{m}^2\text{K})$. Since the test is performed indoors, a heat transfer coefficient for air $h_o = 2.5 \text{ W}/(\text{m}^2\text{K})$ has been used, which deviates from the value used for simulations as given in Table 1. [4]

4.3 Filling tests

After the numerical models were sufficiently developed, the physical system was assembled and used for testing. The test was performed at Propulse NTNU's test facilities at Sandmoen, Trondheim. Due to the possibility of oxygen displacement when testing with gaseous nitrogen, the test setup was placed inside a shipping container with open doors. This provided adequate venting and reduced the risk of asphyxiation. The ambient temperature was 10.5 °C with slight wind gusts.

The test setup is similar to the setup that will be used to fill the rocket. Importantly, Figure 12 shows the fitting assembly on top of the COPV with thermocouple placements. Note that none of the thermocouples are inside the COPV, but rather in the gas stream going into the COPV. Since the COPV only has an opening in one end, it is impossible to measure both the inner wall temperature and gas temperature inside the tank. This affects the results significantly, as seen in Figure 17. Further discussion is provided in section 6.

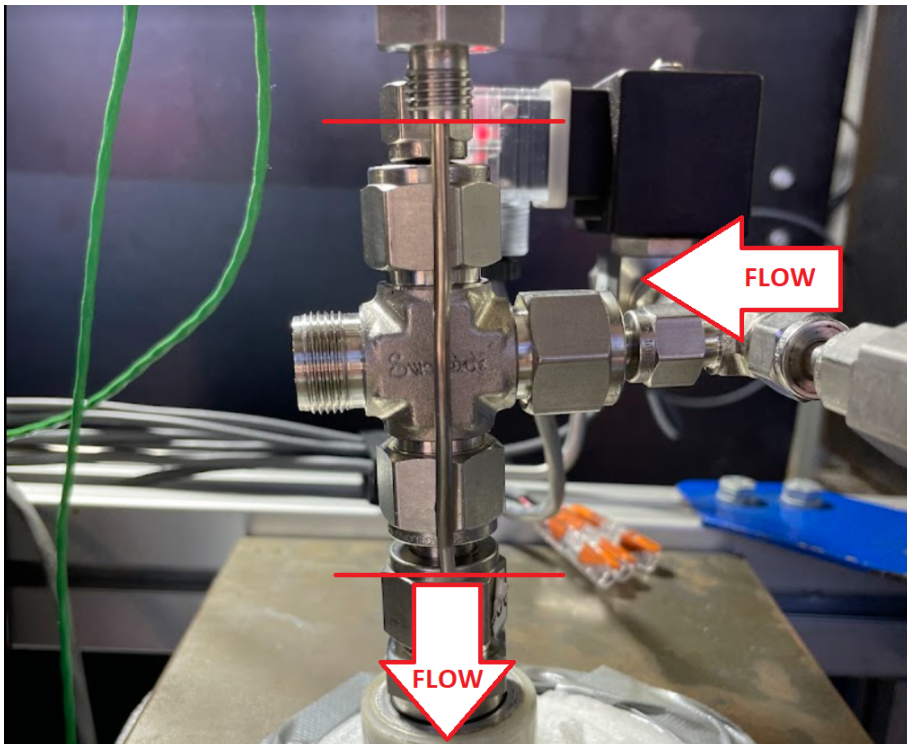


Figure 12: Fitting assembly on top of the COPV. Flow directions are marked with white and red arrows. Horizontal red lines indicate insertion depth of the 100 mm thermocouple probe.

In total, three attempts were required to achieve a successful test due to minor technical difficulties. As a result, the initial supply pressures were lower than the simulated values for the final test. Measurements indicated that the initial LP supply pressure was 151 bar, and the HP supply pressure was 254 bar.

The formulae developed in section 2.4.3 can be used to determine the temperature profile through the wall by using the measured outer wall temperature as a boundary condition for the FDM model. This eliminates the effects of the mass flow model on

the thermal model. These results will be referred to as the test-based FDM results.

In order to estimate the gas temperature, it is necessary to find the gas mass as a function of time as well. The gas mass and the gas temperature will be found by solving a non-linear set of equations. The first equation is given by equation (1),

$$P_{k+1}V - m_{k+1}R_s T_{k+1}^g = 0. \quad (38)$$

The second equation is given by equation (25),

$$T_k^g - \Delta t \frac{h_g A (T_k^g - T_k^0)}{m_k c_V} + \frac{(m_{k+1} - m_k)}{m_k} T_k^g - T_{k+1}^g = 0. \quad (39)$$

The two equations are solved simultaneously using `scipy.optimize.fsolve`. The inner boundary temperature is given by equation (31) and the temperature of the internal nodes are given by equation (29).

5 Results

5.1 Ideal simulation results

This section will present the simulation results for all models with ideal parameters. The initial HP and LP supply pressures are 300 bars and 200 bars, respectively, and ambient the temperature is 20 °C.

5.1.1 Thermal resistances

The results from the thermal resistance model described in section 2.2.1 with ideal initial conditions is shown in Figure 13. The temperature of both the gas and the wall layers rapidly spikes to approximately 80 °C, then drops quickly to a little over 25 °C, before spiking again to about 60 °C when the HP supply opens. These temperature fluctuations occur more rapidly compared to other models. Additionally, the pressure in the COPV increases slower than in the other models. The filling duration is 200 seconds and the system reaches equilibrium after 250 seconds. Note that when the mass flow is linear, the flow is critical.

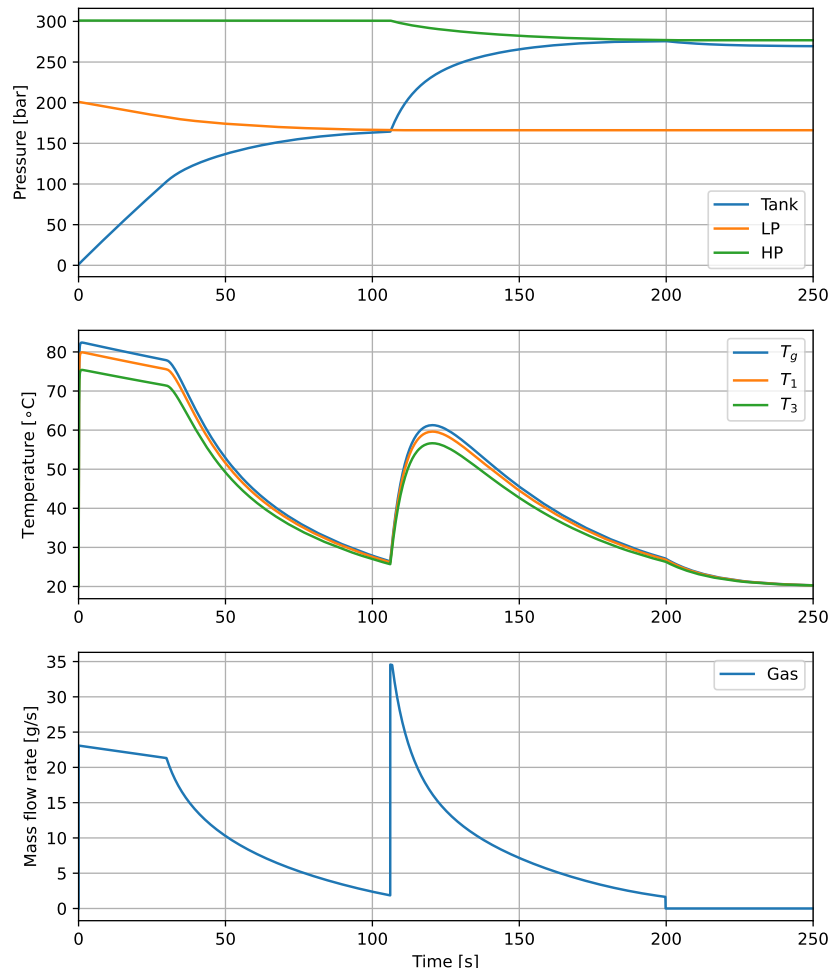


Figure 13: Thermal resistance simulation results.

5.1.2 FDM

Eight nodes are used for the FDM simulations. Two simulations have been performed using the FDM model: one simulation with a convective outer boundary, shown in Figure 14, and one simulation with an adiabatic outer boundary.

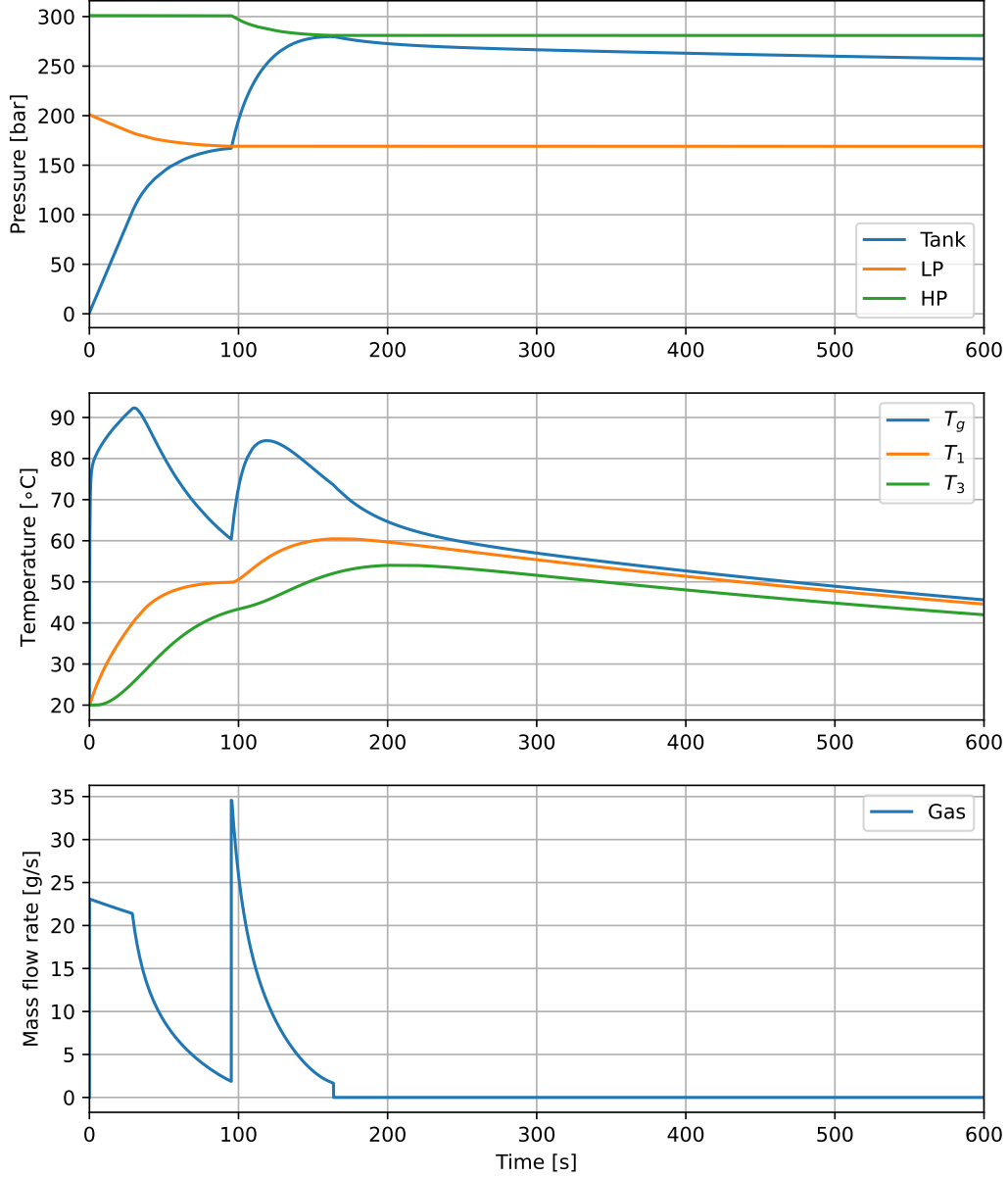


Figure 14: FDM simulation results with a convective outer boundary.

Similarly to the resistance model, the gas temperature quickly spike to a little over 90 $^{\circ}$ C. However, the wall temperatures increase more gradually and peak after the tank filling is complete. The pressure in the COPV rises slightly faster than in the resistance model. Additionally, the pressure drops more significantly after the tank filling is complete, stabilizing at a little over 250 bar. The flow is critical in the start of the simulation, just like in the resistance model. When the simulation is conducted with an adiabatic outer wall, the tank reach a thermal equilibrium at 65 $^{\circ}$ C after 300 seconds.

5.1.3 Simulink Simscape Fluids

The Simulink model results is shown in Figure 15. The filling duration is 200 seconds, which is very close to the duration predicted by the resistance model. However, the temperature profile differs, and coincide closer with the temperatures predicted by the FDM model. The mass flow is consistently lower than the two other models. Note that for the Simulink model, dm/dt is continuous during the filling from LP supply, indicating that the flow is subcritical.

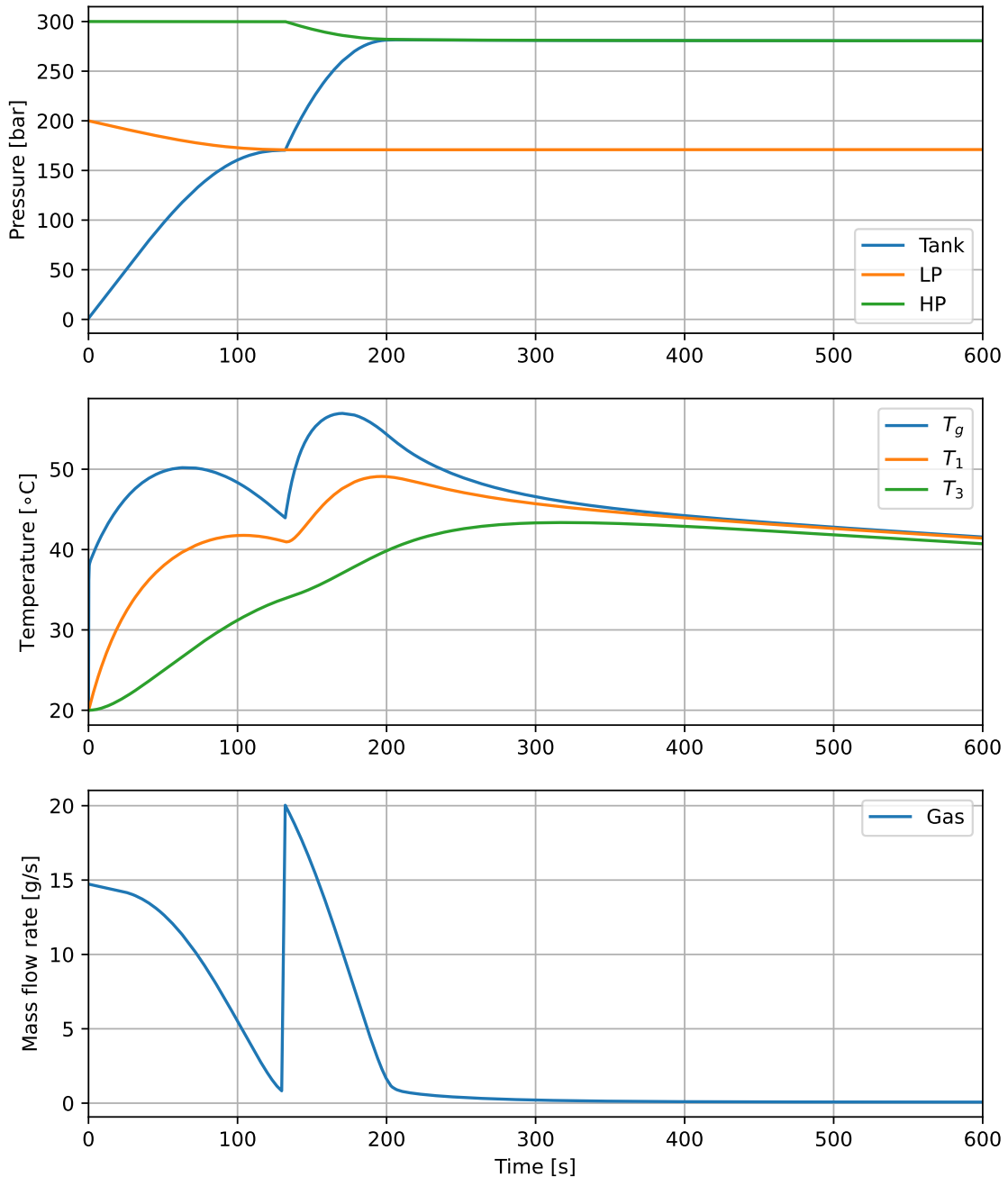


Figure 15: Simulink simulation results.

5.2 Test results

This section presents the results from the tests described in section 4. The comparison between the filling verification test and the simulation results is presented later in section 6.1.

5.2.1 Contact resistance

The data from the test described in section 4.2 is shown in Figure 16. In a steady state, the temperature difference between the water and the outside of the wall was measured to be 5 °C.

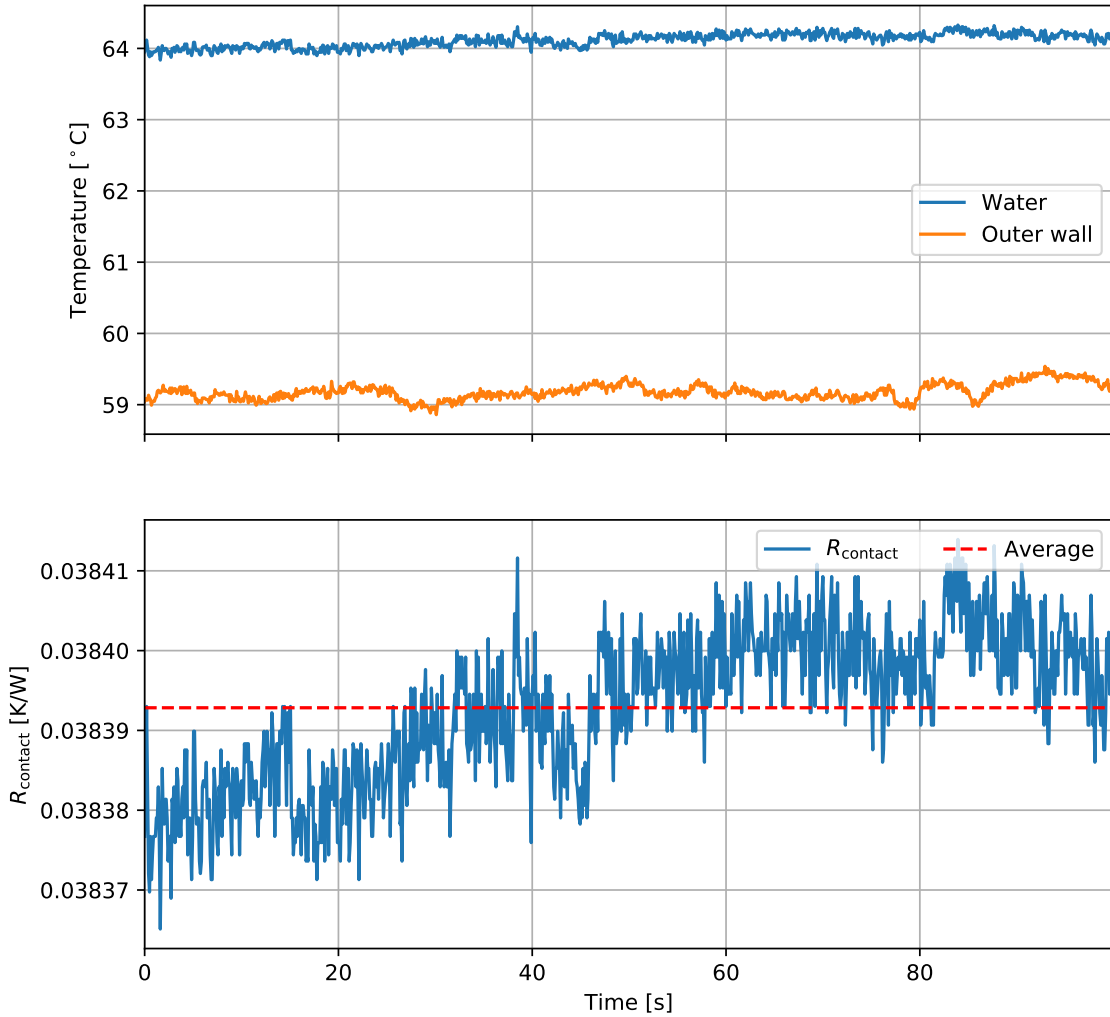


Figure 16: Results from the steady state resistance test.

The contact resistance was calculated for each data point shown in Figure 16. The average contact resistance, $R_{\text{contact}} = (0.038 \pm 0.001)$ K/W, is used as the final result from the test.

5.2.2 Filling test

The results from the test described in section 4.3 are shown in Figure 17. The fluctuations in the first outer wall temperature measurement comes from wind gusts passing through the test area. The second outer wall thermocouple is mounted on the back side of the tank, and is therefore not affected by winds to the same extent.

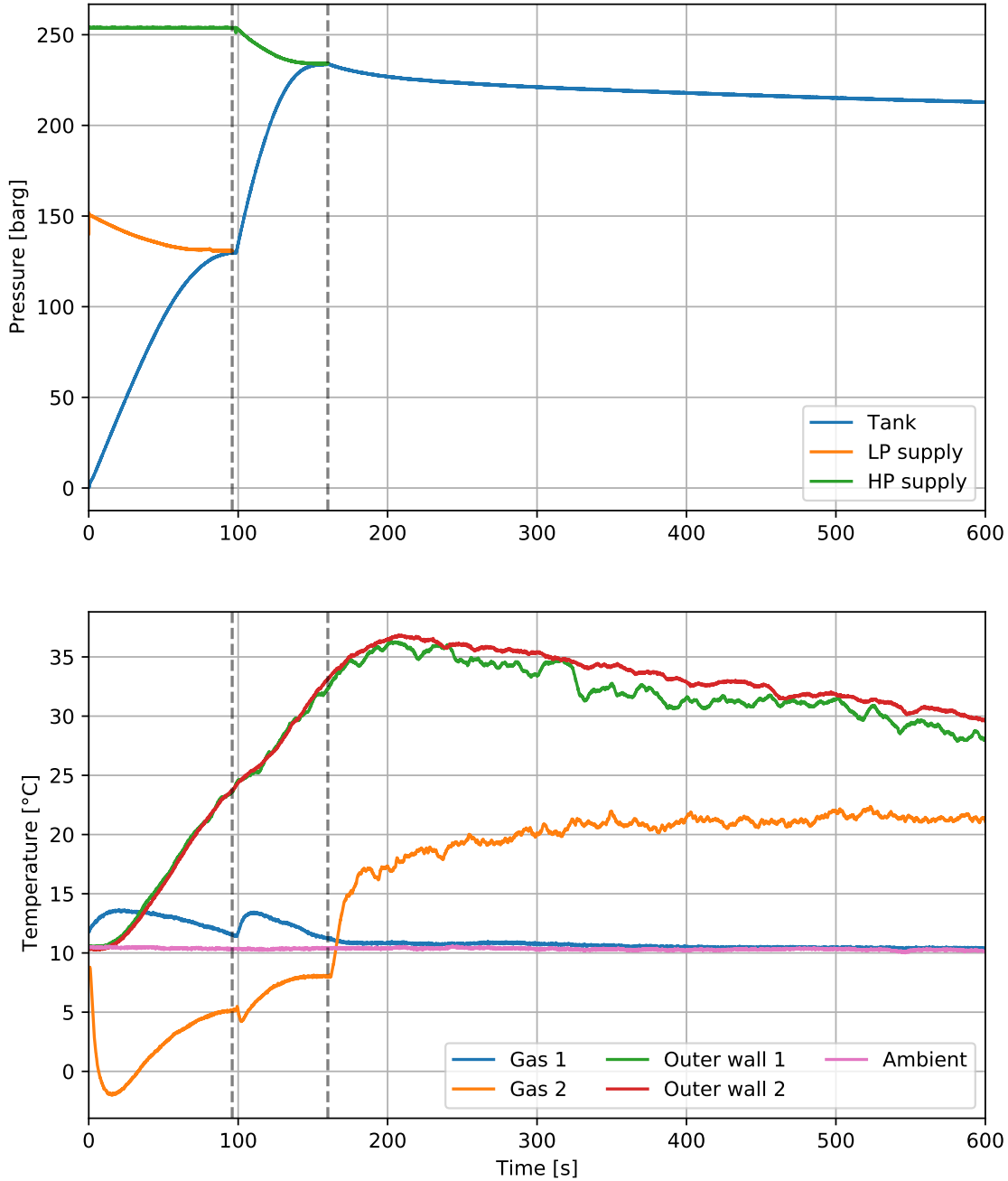


Figure 17: Measured data from the filling test. The vertical lines indicate when the LP and HP valves are closed. The thermocouples with probe lengths 10 mm and 100 mm are labeled Gas 1 and Gas 2, respectively.

The sensor that was not placed directly in the gas stream, labeled Gas 1, only measured a small increase in temperature before returning to ambient when the filling process ended. The temperature measured by the sensor placed inside the gas stream, labeled Gas 2, decreased and stayed below the ambient temperature during the entire filling process.

Figure 18 shows the calculated gas temperature and node temperatures found using the FDM model as described in section 4.3. Note that the Outer wall 2 measurement in Figure 17 and the Node 8 temperature in Figure 18 are the same.

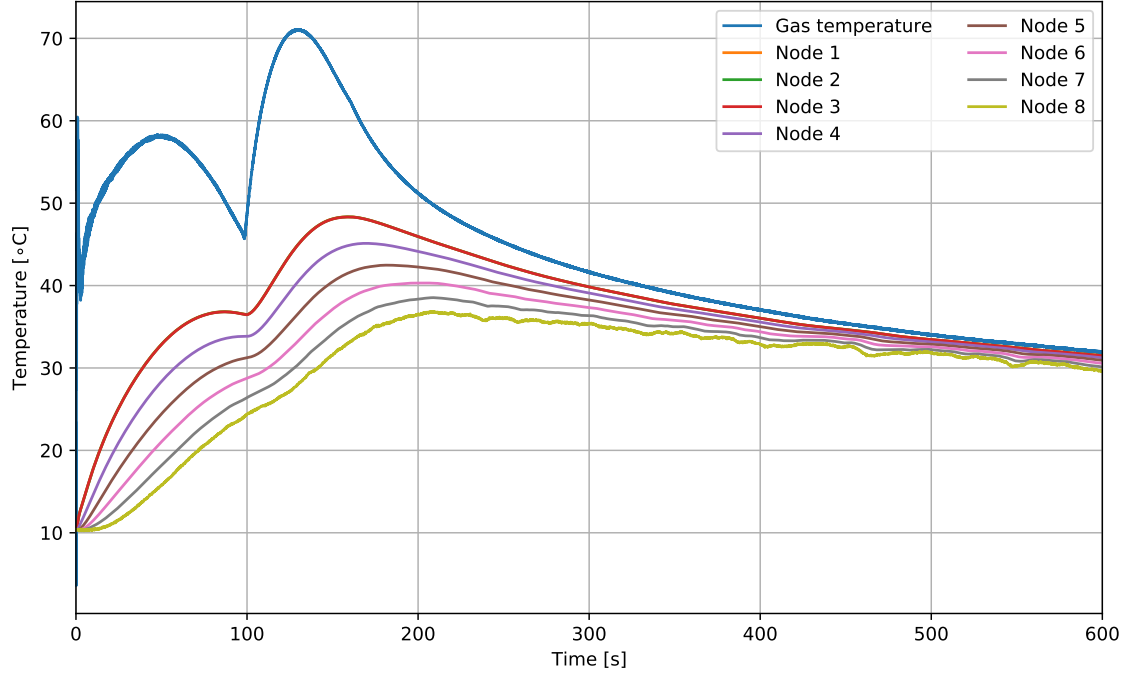


Figure 18: Test based FDM results. Node 8 is given by Outer wall 2 in Figure 17.
Node 1, 2, and 3 are overlapping.

This results in a much more plausible gas temperature than the one measured in the test. In addition to this, it gives a good distribution of node temperatures in the wall that can be compared with the simulation models.

6 Discussion

6.1 Numerical model comparison

The thermal resistance model does not yield accurate results. The heat transfer through the wall seems too high as the wall temperatures follows the temperature of the gas closely. This is likely due to the transient nature of the system being simulated as the base assumption for the model is steady conditions. Another consequence of this is that the simulation does not converge with diminishing time steps. It is worth noting that even though the temperature is unrealistic and contradictory to empirical results, the pressure and mass development is similar to the other models.

Recall that T_1 represents the inner wall temperature and T_3 the outer wall temperature. Results for T_g , T_1 , and T_3 from both the test-based FDM, simulation FDM, as well as the Simulink model, are presented in Figure 19.

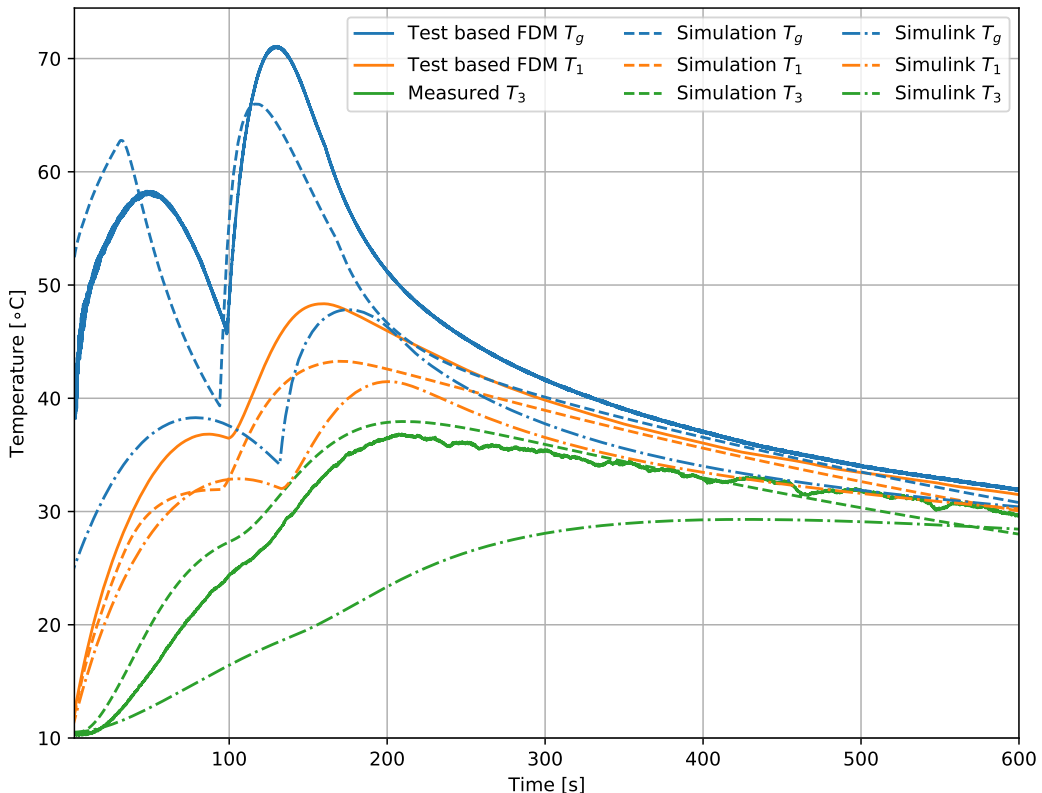


Figure 19: Comparison between models. The solid green line is a physical measurement (see section 5.2), while the other lines are generated using the models.

Analysis of Figure 19 reveals that the FDM simulation, incorporating both mass flow and heat flow simulations, most accurately predicts the outer wall temperature. The Simulink model follows the same general shape, but is offset by up to 13 °C. Notably, the Simulink model yields a significantly lower outer wall temperature, suggesting a higher heat flow rate through the wrapping. This effect is likely exacerbated by an underestimation of the gas temperature.

The FDM simulation and the test-based FDM yield similar results for the two wall temperatures, as shown in figures 19 and 20 , suggesting that any differences between them could likely be minimized by more accurately determined physical properties of the COPV. However, there is a noticeable discrepancy in the estimated gas temperatures for the two models. It is possible that the thermal model is more precise than the mass flow model.

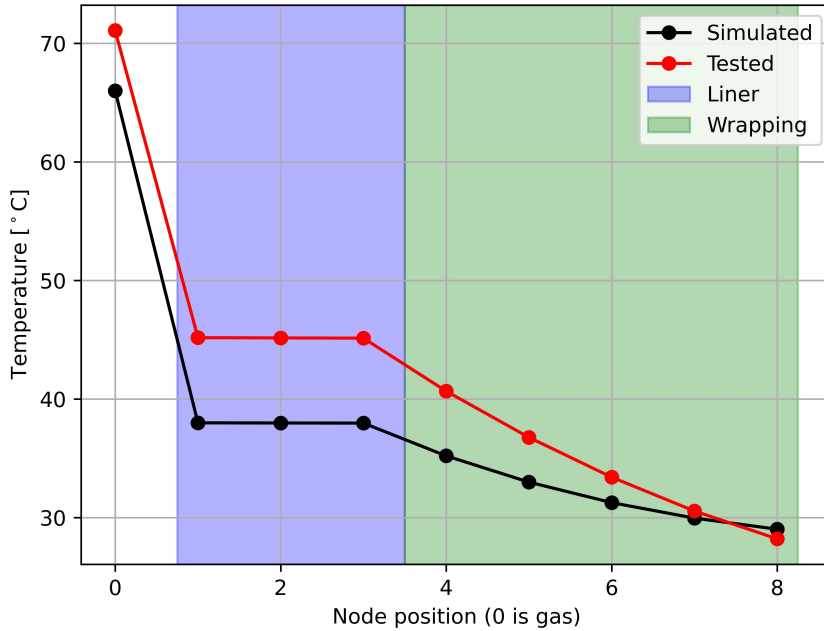


Figure 20: Comparison of test-based FDM and FDM simulation when the gas is at its maximum temperature.

During large transients, the FDM simulation tends to overestimate gas temperatures. This is due to the slower convection from the gas to the inner wall compared to the addition of more mass inside the tank. If possible, by placing a thermocouple on the inner wall, as well as accurately measuring the temperature of the gas inside the tank, data could have been gathered and used as a basis for a quantitative comparison between the different models and the test results.

In both the ideal simulations and the simulations with initial conditions based on test measurements, the Simulink model results show a noticeably longer duration for the entire filling process compared to the other models. This is one of the contributing reasons to why the gas temperature is lower with this model.

There are many factors present in the real system that are not present in the simulations. For instance, the pipes and supply tanks modeled as isentropic, while in reality a lot of energy is potentially lost in the piping. The wall of the tank, which is modeled as homogeneous, is in reality made from wound carbon fibers that are inhomogeneous and are more conductive in the direction parallel of the fibers. Thus, it is likely that all of the thermal models estimate the heat transfer through the wrapping incorrectly. If the fiber type and epoxy type had been known, it would be possible to more accurately determine the conductivity and specific heat, as done in [9].

6.2 Numerical simulations

A constant time step is used in this thesis. It is natural to extend the custom simulation program to incorporate adaptive time steps. There are many benefits to this, including shorter run time and smaller data files. A method for adaptive step control for transient thermal analysis is given in [10]. Nevertheless, the stability criteria given by equation (35) yields sufficient results with a total runtime of only one second.

A natural improvement to the custom simulator is to solve for the gas properties implicitly, including mass, temperature, and pressure. Since the heat transfer through the wall is a slower process, it is unlikely that computing the temperature distribution implicitly would have any major effect on the results. Combined with an adaptive step size, it is possible to achieve stable simulations, even during rapid transients, without a waste of computing power or prolonged runtime.

6.3 Contact resistance test

The contact resistance $R_{\text{contact}} = (0.038 \pm 0.001) \text{ K/W}$ is higher than common values found in literature. [4] This is likely because one of the other resistances in the system is estimated to be too low, causing the calculation of the contact resistance to be too high. An incorrect estimate of the heat transfer coefficient for water h_{water} could be the source of this error. The heat transfer coefficient for forced convection of liquids varies a lot depending on the liquid, and since it is difficult to place a sensor on the inside wall to measure the inner wall temperature, it is not possible to empirically determine it. The test otherwise gave a lot of insight into how the temperature on the outside wall of the tank developed as the tank was filled with a warm fluid.

6.4 Filling test

The recorded gas temperatures from both sensors contradicted the expectation that the gas temperature would increase and stay above the wall temperature. Neither of the sensor readings increased as much as simulated, and the one inside the gas stream decreased below ambient during the transient phase of the test. These measurements can be explained by the placement of the sensors. The sensor in the gas stream was placed at the throat of the tank, not inside the tank. This means that it measured the temperature of the gas as it expanded from the piping and into the tank, where the gas is cooling down, instead of where it got compressed and heated up inside the tank. This is supported by the significant increase in temperature after the transient filling process is done, and the temperature sensor can be heated up by the warmer gas in the tank.

The sensor not exposed to the gas stream only experienced a slight increase in temperature during the test's transient phase and quickly returned to the ambient temperature once the filling was complete. This behavior can be attributed to the sensor

housing's significant thermal mass and low thermal conductivity. Unlike the external wall sensors, the sensors measuring the gas are encased within an Inconel 600 housing that screws into the piping and withstands internal pressure. This housing substantially increases the sensor's thermal mass, and when combined with the slow heat transfer via natural convection from the gas, the sensor's temperature rise was minimal compared to that of the gas, resulting in inaccurate measurements. The same logic can be applied to explain why the sensor in the gas stream didn't measure a higher temperature after the transient phase of the test. The sensor in the gas stream would measure a temperature closer to the real temperature of the gas because the convective heat transfer from the gas to the sensor was forced until the system is no longer transient, where the temperature stops changing.

A better FDM analysis of the temperatures inside the wall could have been done if the temperature of the gas in the tank had been measured accurately. A good gas temperature measurement together with a good measurement of the temperature of the inner wall is needed to more accurately determine the material properties of the tank.

The temperature measurements on the outside of the tank matched the expectation more closely. This is because the sensors mounted to the wall do not share many the same issues as discussed with the gas temperature sensors. The two sensors measure a similar temperature, however one of the sensors fluctuated a lot more than the other. Since it only fluctuated downward, this likely is because the sensor was more exposed to wind passing through the test area. It is likely that this sensor experienced forced convection due to the wind gusts, whilst the other sensor experienced natural convection, leading to more heat being transferred away.

7 Conclusion

In this thesis, several modelling and simulation approaches have been developed and investigated with use on a system encompassing the filling of a COPV using high pressure gaseous nitrogen.

The FDM model aligns closely with empirical results, particularly regarding the outer wall temperature. Considering the critical importance of maintaining temperatures within designed limits, the development of an accurate simulation tool using FDM enables the prediction of these temperatures without the need for initial tests. It is not possible to quantitatively define the accuracy of the mass flow model in conjunction with the FDM thermal model without a precise measurement of either the gas temperature or the inner wall temperature. Nevertheless, there are similarities between the gas temperature in these simulations and in the results from [1].

Even though the mass flow model coincides with empirical data, it should be further developed to improve its accuracy. The energy and pressure losses in pipes should be accounted for, as described in [6]. The custom simulator currently only handles one restriction for each tank, which reduces its flexibility and the number of systems it can accurately model. It is beneficial to develop formulae for multiple restrictions, both in parallel and in series, in order to broaden its capabilities.

The supply tanks were modeled as adiabatic, which proved to be sufficient for the system modelled in this thesis. Nevertheless, extending the custom simulator to include FDM models for all tanks is a natural path for further work. It can be done in simple terms by moving the functions that update the temperature away from the solver class and into the tank class. The tank simulation can also be improved by expanding it to two dimensions as done in [1]. However, the same source states that simulating only one dimension is sufficient as the temperature of the wall is very similar across the whole surface of the COPV.

More testing should be done to accurately determine the properties of the wall of the tank to improve the accuracy of the simulation. A repeat of the filling experiment with a temperature sensor inside the tank to measure the gas temperature, and if possible a sensor on the inside wall could provide valuable data to empirically determine how heat is transferred through the wall.

The empirical data showed that the wall temperature does not reach above the limit of 65 °C during the filling process by using carefully chosen restriction orifices. This result is also predicted accurately by the finite difference model, meaning it can be utilized to simulate Propulse NTNU's future systems only requiring minor improvements.

Bibliography

- [1] Y. Jiang, ‘Influences of filling process on the thermal-mechanical behavior of composite overwrapped pressure vessel for hydrogen’, International Journal of Hydrogen Energy 45, DOI:10.1016/j.ijhydene.2020.06.154 (2020).
- [2] NASA, *Advances in understanding copv structural life*, <https://www.nasa.gov/centers-and-facilities/nesc/advances-in-understanding-copv-structural-life/> (visited on 26th Apr. 2024).
- [3] ISO 11119-12:2020(E), *Gas cylinders — design, construction and testing of refillable composite gas cylinders and tubes - part 2: fully wrapped fibre reinforced composite gas cylinders and tubes up to 450 l with load-sharing metal liners*, 3rd edition (International Organization for Standardization, Vernier, Geneva, Switzerland).
- [4] Y. A. ÇENGEL, *Heat and mass transfer. fundamentals applications* (McGraw-Hill Education, 2020).
- [5] ISO 5167-1:2022(E), *Measurement of fluid flow by means of pressure differential devices inserted in circular cross-section conduits running full — part 1: general principles and requirements*, 3rd edition (International Organization for Standardization, Vernier, Geneva, Switzerland).
- [6] Committee for the Prevention of Disasters, *Methods for the calculation of physical effects due to releases of hazardous materials (liquids and gases)*, 2nd edition (The Hague, Ministre van Verkeer en Waterstaat, 2005).
- [7] P. C. Hemmer, *Termisk fysikk*, 2nd edition (Tapir akademisk forlag, 2002).
- [8] J. Lee, ‘Stability of finite difference schemes on the diffusion equation with discontinuous coefficients’, (2017).
- [9] R. J. et al, ‘Thermal properties of carbon fiber-epoxy composites with different fabric weaves’, International SAMPE Technical Conference (2012).
- [10] R. V. MOHAN, ‘Finite element/finite volume approaches with adaptive time stepping strategies for transient thermal problems’, Sādhanā 19, <https://doi.org/10.1007/BF02744404> (1994).
- [11] E. Kreyszig, *Advanced engineering mathematics*, 10th edition (John Wiley Sons Inc, 2011).
- [12] K. Rottmann, *Matematisk Formelsamling* (Universitetsforlaget, 2019).

Appendix

A Wall area estimation

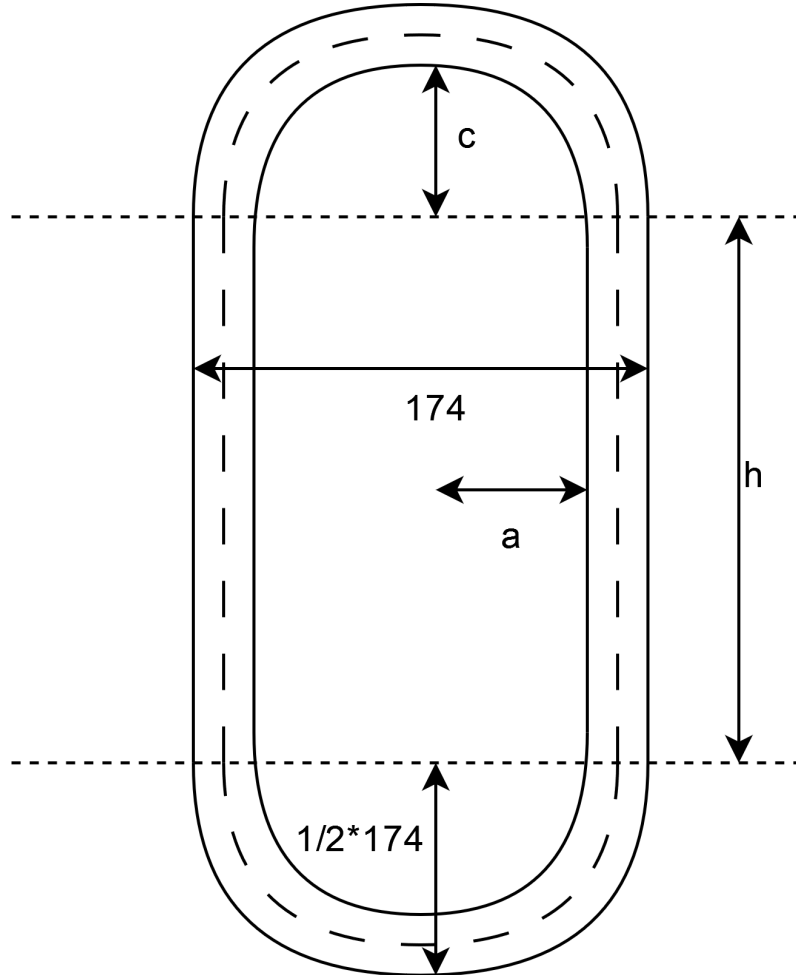


Figure 21: Cross-sectional view of the tank with geometrical dimensions.

Figure 21 shows a cross-sectional view of the tank. The total end-cap volume is then given by the volume of one spheroid,

$$V_s = \frac{4}{3}a^2c \quad (40)$$

where a is the semi-major axis and c the semi-minor axis, as indicated in Figure 21. A common value for c is $a/2$, which will be assumed going forward. The height of the cylinder h is then

$$h = \frac{1}{\pi a^2} \left(V_{\text{tank}} - \frac{2}{3}a^3 \right). \quad (41)$$

To find the surface area of the spheroid, it is first necessary to find its eccentricity, which is

$$e^2 = 1 - \frac{c^2}{a^2} = 1 - \frac{1}{4} = 0.75. \quad (42)$$

The surface area of the spheroid is given by [12] to be

$$A_s = 2\pi a^2 \left(1 + \frac{1-e^2}{e} \operatorname{arctanh} e \right) \quad (43)$$

The total surface area is

$$\begin{aligned} A &= 2\pi ah + 2\pi a^2 \left(1 + \frac{1-e^2}{e} \operatorname{arctanh} e \right) \\ &= \frac{2}{a} \left(V_{\text{tank}} - \frac{2}{3}a^3 \right) + 2\pi a^2 \left(1 + \frac{1-e^2}{e} \operatorname{arctanh} e \right) \\ &\approx \frac{2}{a} \left(V_{\text{tank}} - \frac{2}{3}a^3 \right) + 1.38 \cdot 2\pi a^2 \end{aligned} \quad (44)$$

Using the liner thickness L_{liner} , the liner end-cap volume is

$$V_{s,\text{liner}} = \frac{2}{3} [(a + L_{\text{liner}})^3 - a^3] \quad (45)$$

and the liner cylinder volume is

$$V_{c,\text{liner}} = \pi h [(a + L_{\text{liner}})^2 - a^2] \quad (46)$$

which gives a total liner volume

$$\begin{aligned} V_{\text{liner}} &= \frac{2}{3} [(a + L_{\text{liner}})^3 - a^3] \\ &\quad + \frac{(a + L_{\text{liner}})^2 - a^2}{a^2} \left(V_{\text{tank}} - \frac{2}{3}a^3 \right). \end{aligned} \quad (47)$$

By multiplying with the density of the liner material one can find the thermal mass of the liner. The total tank mass is given in the datasheet, and from this one can easily find the thermal mass of the wrapping as well. The outer diameter (OD) is given in the datasheet, which gives the expression for a ,

$$a = \frac{1}{2} \text{OD} - t_{\text{liner}} - t_{\text{wrapping}}. \quad (48)$$